nature medicine

SUPPLEMENTARY INFORMATION

https://doi.org/10.1038/s41591-018-0071-1

In the format provided by the authors and unedited.

Poly(GR) impairs protein translation and stress granule dynamics in *C9orf72*-associated frontotemporal dementia and amyotrophic lateral sclerosis

Yong-Jie Zhang[1,2], Tania F. Gendron[1,2], Mark T. W. Ebbert[1], Aliesha D. O'Raw[1], Mei Yue[1], Karen Jansen-West[1], Xu Zhang[3], Mercedes Prudencio[1,2], Jeannie Chew[1,2], Casey N. Cook[1,2], Lillian M. Daughrity[1], Jimei Tong[1], Yuping Song[1], Sarah R. Pickles[1], Monica Castanedes-Casey[1], Aishe Kurti[1], Rosa Rademakers[1,2], Bjorn Oskarsson[4], Dennis W. Dickson[1,2], Wenqian Hu[3], Aaron D. Gitler[5], John D. Fryer[1,2] and Leonard Petrucelli[1,2]*

[1]Department of Neuroscience, Mayo Clinic, Jacksonville, FL, USA. [2]Neurobiology of Disease Graduate Program, Mayo Graduate School, Mayo Clinic College of Medicine, Rochester, MN, USA. [3]Department of Biochemistry and Molecular Biology, Mayo Clinic, Rochester, MN, USA. [4]Department of Neurology, Mayo Clinic, Jacksonville, FL, USA. [5]Department of Genetics, Stanford University School of Medicine, Stanford, CA, USA.
*e-mail: petrucelli.leonard@mayo.edu

Poly(GR) impairs protein translation and stress granule dynamics in *C9orf72*-associated frontotemporal dementia and amyotrophic lateral sclerosis

Authors: Yong-Jie Zhang[1,2], Tania F. Gendron[1,2], Mark T. W. Ebbert[1], Aliesha D. O'Raw[1], Mei Yue[1], Karen Jansen-West[1], Xu Zhang[3], Mercedes Prudencio[1,2], Jeannie Chew[1,2], Casey N. Cook[1,2], Lillian M. Daughrity[1], Jimei Tong[1], Yuping Song[1], Sarah R. Pickles[1], Monica Castanedes-Casey[1], Aishe Kurti[1], Rosa Rademakers[1,2], Bjorn Oskarsson[4], Dennis W. Dickson[1,2], Wenqian Hu[3], Aaron D. Gitler[5], John D. Fryer[1,2], Leonard Petrucelli[1,2,*]

Affiliations:

[1]Department of Neuroscience, Mayo Clinic, 4500 San Pablo Road, Jacksonville, Florida 32224, USA.

[2]Neurobiology of Disease Graduate Program, Mayo Graduate School, Mayo Clinic College of Medicine, Rochester, Minnesota 55905, USA.

[3]Department of Biochemistry and Molecular Biology, Mayo Clinic, Rochester, Minnesota 55905, USA.

[4]Department of Neurology, Mayo Clinic, 4500 San Pablo Road, Jacksonville FL 32224, USA.

[5]Department of Genetics, Stanford University School of Medicine, Stanford, California 94305, USA.

*__Correspondence to__:

Leonard Petrucelli, Ph.D.

Department of Research, Neuroscience

Mayo Clinic College of Medicine

4500 San Pablo road

Jacksonville, FL 32224

Office: 1-904-953-2855

Fax: 1-904-953-6276

e-mail: petrucelli.leonard@mayo.edu

Supplementary Discussion

Here, we show that mice expressing GFP-$(GR)_{100}$ throughout the brain developed age-dependent neuron loss, as well as impaired motor and memory skills. In fact, compared to AAV1-GFP-$(GA)_{50}$ mice, the characterization of which was previously reported[32], GFP-$(GR)_{100}$ mice exhibited an earlier disease onset and developed more severe neurodegeneration. Whereas 1.5-month-old GFP-$(GR)_{100}$ mice exhibited brain atrophy, neuron loss and gliosis, no such abnormalities were present in age-matched GFP-$(GA)_{50}$ mice. GFP-$(GA)_{50}$ mice did have a reduced brain weight at 6 months of age (334.7 ± 4.339 mg), but an even greater reduction in brain weight was observed in 6 month-old GFP-$(GR)_{100}$ mice (274.8 ± 9.245 mg; $P < 0.0001$, two-tailed unpaired t test). These findings are consistent with previous studies demonstrating that poly(GR) is more toxic than poly(GA)[33].

The observed neurodegeneration and behavioral deficits in GFP-$(GR)_{100}$ mice were accompanied by the colocalization of cytoplasmic poly(GR) with ribosomal subunits and the translation initiation factor eIF3η, which was also observed in the cortex of c9FTD/ALS patients. Given that TDP-43 pathology is a hallmark feature of c9FTD/ALS, we also examined whether poly(GR) expression causes such pathology. Inclusions of phosphorylated TDP-43 were rarely observed in GFP-$(GR)_{100}$ mice (only ~1–3 cells per sagittal hemibrain section showed TDP-43 pathology; **Supplementary Fig. 11a**). In contrast, frequent phosphorylated TDP-43 inclusions were seen in mice expressing $(G_4C_2)_{66}$, which produced G_4C_2 RNA foci and DPR proteins[27], suggesting that induction of TDP-43 pathology requires G_4C_2 RNA or aggregated DPR proteins. *C9orf72* repeat expansions are also reported to disrupt nucleocytoplasmic trafficking by impairing nuclear membrane integrity and the localization of RanGAP1[4,17,24,32]. Staining for lamins A/C and B1 revealed no defects in nuclear envelope integrity, nor was

RanGAP1 mislocalized in poly(GR)-positive cells in comparison to poly(GR)-negative cells (**Supplementary Fig. 11b**). These findings are in line with a study showing a normal distribution of RanGAP1 and Lamin B1 in poly(GR)-positive cells of the motor cortex and spinal cord of c9ALS patients[16].

Poly(GR) has additionally been shown to cause nucleolar stress by suppressing ribosomal RNA (rRNA) synthesis[19-21]. While colocalization of poly(GR) and the nuclear marker fibrillarin was observed in HEK293T cells expressing high levels of GFP-$(GR)_{100}$ (**Supplementary Fig. 11c**), poly(GR) did not colocalize with the nucleolar marker fibrillarin in GFP-$(GR)_{100}$ mice (**Supplementary Fig. 11d**), which is consistent with the absence of detectable nucleolar poly(GR) in c9FTD/ALS[16,45,46]. Combined with the fact that the expression of rRNAs was not altered in GFP-$(GR)_{100}$ mice (**Supplementary Fig. 11e**,**f**), these data argue against nucleolar poly(GR) playing a role in c9FTD/ALS. Nonetheless, it remains possible that relatively short poly(GR) peptides, difficult to detect by immunohistochemistry, are produced in c9FTD/ALS and cause nucleolar stress.

To examine whether poly(GR) aggregates, TDP-43 pathology, defects in nucleocytoplasmic transport and/or nucleolar stress may have developed in GFP-$(GR)_{100}$ mice prior to 1.5 months of age, and thus contributed to the neuronal loss observed at this this time-point, we examined 1-week-old GFP-$(GR)_{100}$ mice. At this age, GFP-$(GR)_{100}$ mice showed no significant changes in brain weight or gross morphology compared to age-matched GFP mice (**Supplementary Fig. 12a**,**b**). Likewise, no poly(GR) inclusions, TDP-43 pathology, RanGAP1, Lamin B1 or Lamin A/C mislocalization, or nucleolar distribution of poly(GR) were detected (**Supplementary Fig. 12c–f**). Together, these data demonstrate that poly(GR) caused neurodegeneration in vivo independently of TDP-43 pathology, nucleocytoplasmic transport defects, and nucleolar stress.

Supplementary Discussion References

4. Zhang, K., *et al.* The C9orf72 repeat expansion disrupts nucleocytoplasmic transport. *Nature* **525**, 56-61 (2015).
16. Saberi, S., *et al.* Sense-encoded poly-GR dipeptide repeat proteins correlate to neurodegeneration and uniquely co-localize with TDP-43 in dendrites of repeat-expanded C9orf72 amyotrophic lateral sclerosis. *Acta Neuropathol* **135**, 459-474 (2018).
17. Jovicic, A., *et al.* Modifiers of C9orf72 dipeptide repeat toxicity connect nucleocytoplasmic transport defects to FTD/ALS. *Nat Neurosci* **18**, 1226-1229 (2015).
19. Kwon, I., *et al.* Poly-dipeptides encoded by the C9orf72 repeats bind nucleoli, impede RNA biogenesis, and kill cells. *Science* **345**, 1139-1145 (2014).
20. Lee, K.H., *et al.* C9orf72 Dipeptide Repeats Impair the Assembly, Dynamics, and Function of Membrane-Less Organelles. *Cell* **167**, 774-788 e717 (2016).
21. Tao, Z., *et al.* Nucleolar stress and impaired stress granule formation contribute to C9orf72 RAN translation-induced cytotoxicity. *Hum Mol Genet* **24**, 2426-2441 (2015).
24. Freibaum, B.D., *et al.* GGGGCC repeat expansion in C9orf72 compromises nucleocytoplasmic transport. *Nature* **525**, 129-133 (2015).
27. Chew, J., *et al.* Neurodegeneration. C9ORF72 repeat expansions in mice cause TDP-43 pathology, neuronal loss, and behavioral deficits. *Science* **348**, 1151-1154 (2015).
32. Zhang, Y.J., *et al.* C9ORF72 poly(GA) aggregates sequester and impair HR23 and nucleocytoplasmic transport proteins. *Nat Neurosci* **19**, 668-677 (2016).
33. Mizielinska, S., *et al.* C9orf72 repeat expansions cause neurodegeneration in Drosophila through arginine-rich proteins. *Science* **345**, 1192-1194 (2014).
45. Schludi, M.H., *et al.* Distribution of dipeptide repeat proteins in cellular models and C9orf72 mutation cases suggests link to transcriptional silencing. *Acta Neuropathol* (2015).
46. Vatsavayai, S.C., *et al.* Timing and significance of pathological features in C9orf72 expansion-associated frontotemporal dementia. *Brain* **139**, 3202-3216 (2016).

Supplementary Figure 1.

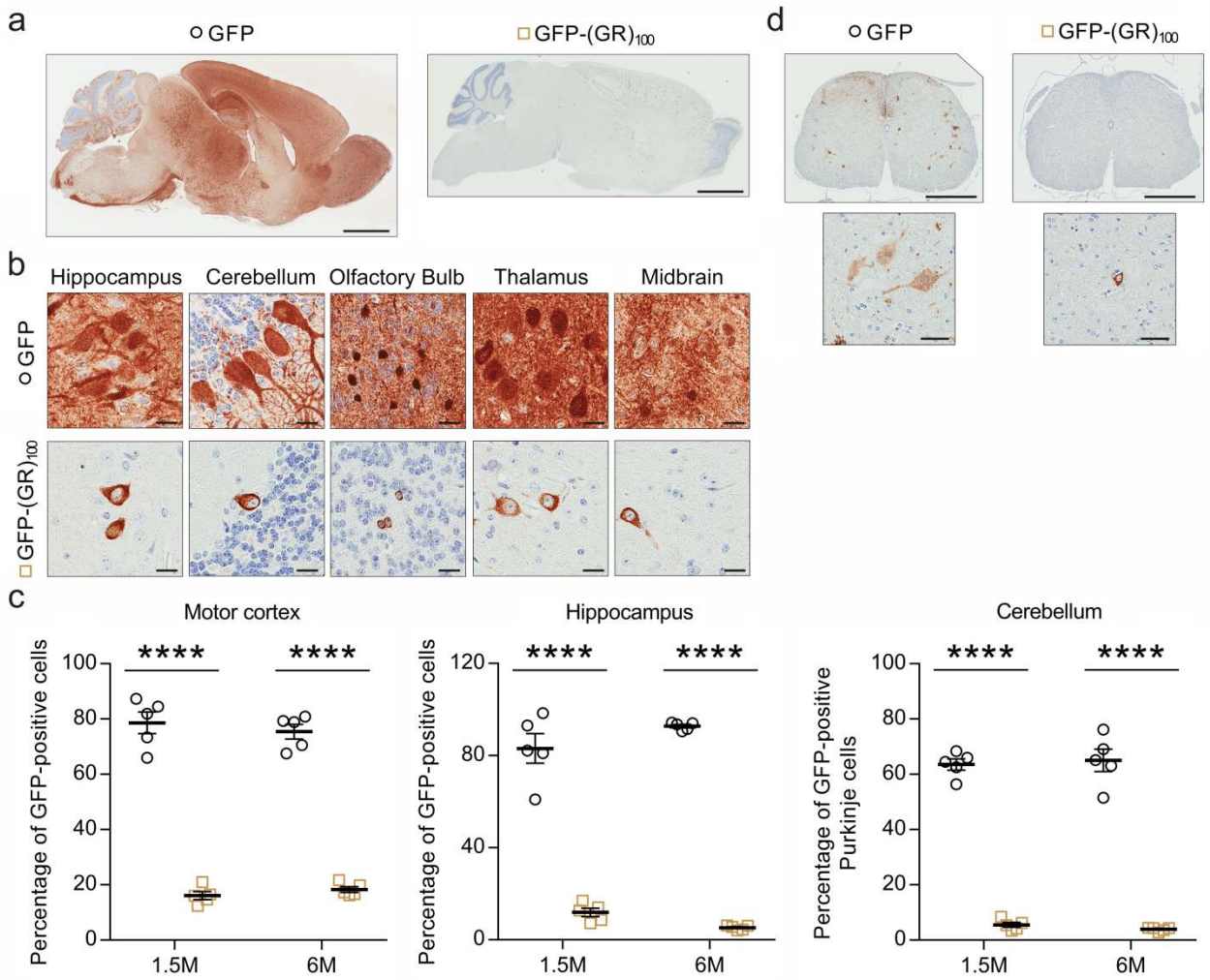

Supplementary Figure 1. Regional distribution of transgene in brains of GFP and GFP-$(GR)_{100}$ mice. (**a**) Gross morphological analysis with GFP staining of brains from 6-month-old mice expressing GFP (n = 12) or GFP-$(GR)_{100}$ (n = 9). Scale bar, 2 mm. (**b**) Immunohistochemical analysis of the indicated brain regions of 6-month-old mice expressing GFP (n = 12) or GFP-$(GR)_{100}$ (n = 9) with anti-GFP antibody. Scale bars, 20 μm. (**c**) Quantification of the percentage of GFP-positive cells in the motor cortex or CA1–CA3 regions of the hippocampus, and GFP-positive Purkinje cells in the cerebellum of 1.5- and 6-month-old GFP and GFP-$(GR)_{100}$ mice (n = 5 per group). (**d**) Immunohistochemical analysis of GFP in the

spinal cord of 6-month-old mice expressing GFP (n = 6) or GFP-$(GR)_{100}$ (n = 5) with anti-GFP antibody. Images of low (top) and high (bottom) magnification are shown. Scale bars, 600 μm (top), 50 μm (bottom). Data are presented as mean±s.e.m. In **c**: **** $P < 0.0001$, two-way ANOVA, Tukey's multiple-comparison test.

Supplementary Figure 2

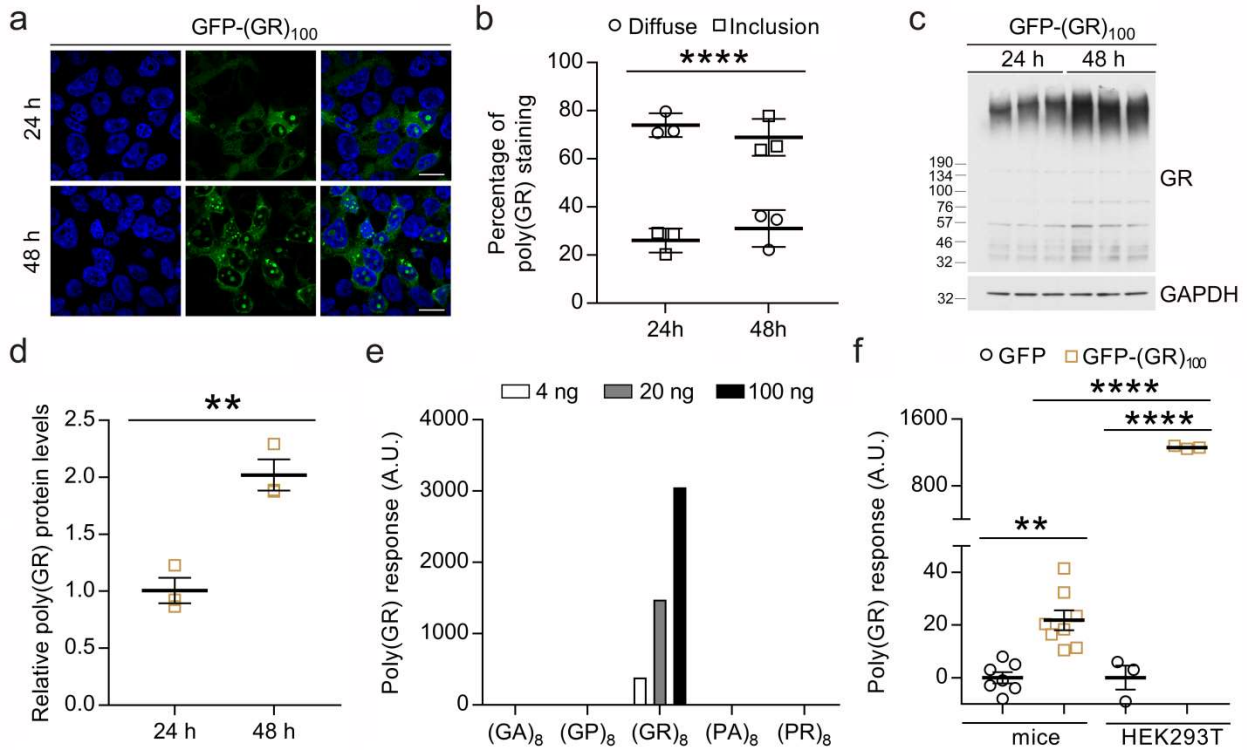

Supplementary Figure 2. Expression of GFP-$(GR)_{100}$ led to the formation of cytoplasmic aggregates in a time- and concentration-dependent manner. (**a**,**b**) Representative images (**a**) and quantification (**b**) of HEK293T cells with cytoplasmically diffuse or aggregated GFP-$(GR)_{100}$ 24 or 48 h post-transfection (n = 3 independent experiments). Scale bars, 10 μm. (**c**,**d**) Immunoblots (**c**) and densitometric analysis of immunoblots (**d**) to examine protein levels of GFP-$(GR)_{100}$ in HEK293T cells expressing GFP-$(GR)_{100}$ 24 or 48 h post-transfection (n = 3 independent experiments). (**e**) An immunoassay for poly(GR) was developed that detects poly(GR) peptides but not peptides representing the other DPRs RAN translated from the *C9orf72* repeat expansion. (**f**) The poly(GR) immunoassay was used to measure poly(GR) in the cortex and hippocampus of 6-month-old mice expressing GFP (n = 7) or GFP-$(GR)_{100}$ (n = 8), and in HEK293T cells expressing GFP or GFP-$(GR)_{100}$ 24 h post-transfection (n = 3 independent experiments). Data are presented as mean±s.e.m. In **b**: **** $P < 0.0001$ (24 h inclusion vs. 48 h

inclusion), two-way ANOVA, Tukey's multiple-comparison test. In **d**: ** $P = 0.0046$, two-tailed unpaired t test. In **f**: **** $P < 0.0001$ and ** $P = 0.0037$, one-way ANOVA, Tukey's multiple-comparison test.

Supplementary Figure 3

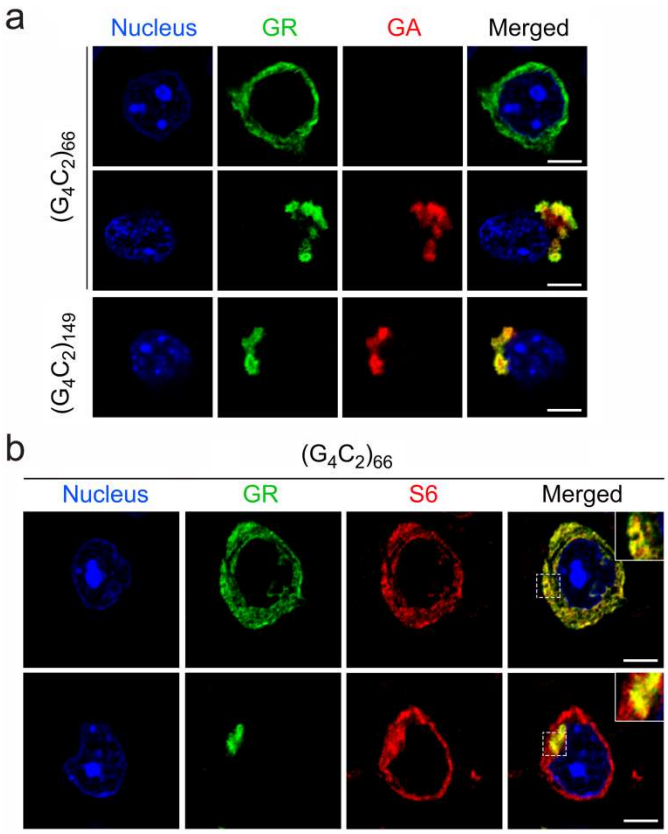

Supplementary Figure 3. Poly(GR) co-localized with poly(GA) and ribosomal proteins in $(G_4C_2)_{66}$ and $(G_4C_2)_{149}$ mice. (**a**) Double-immunofluorescence staining for poly(GR) and poly(GA) in the cortex of 6-month-old $(G_4C_2)_{66}$ and $(G_4C_2)_{149}$ mice (n = 3 per group). (**b**) Double-immunofluorescence staining for poly(GR) and the ribosomal protein S6 in the cortex of 6-month-old $(G_4C_2)_{66}$ mice (n = 3). All scale bars, 5 μm.

Supplementary Figure 4

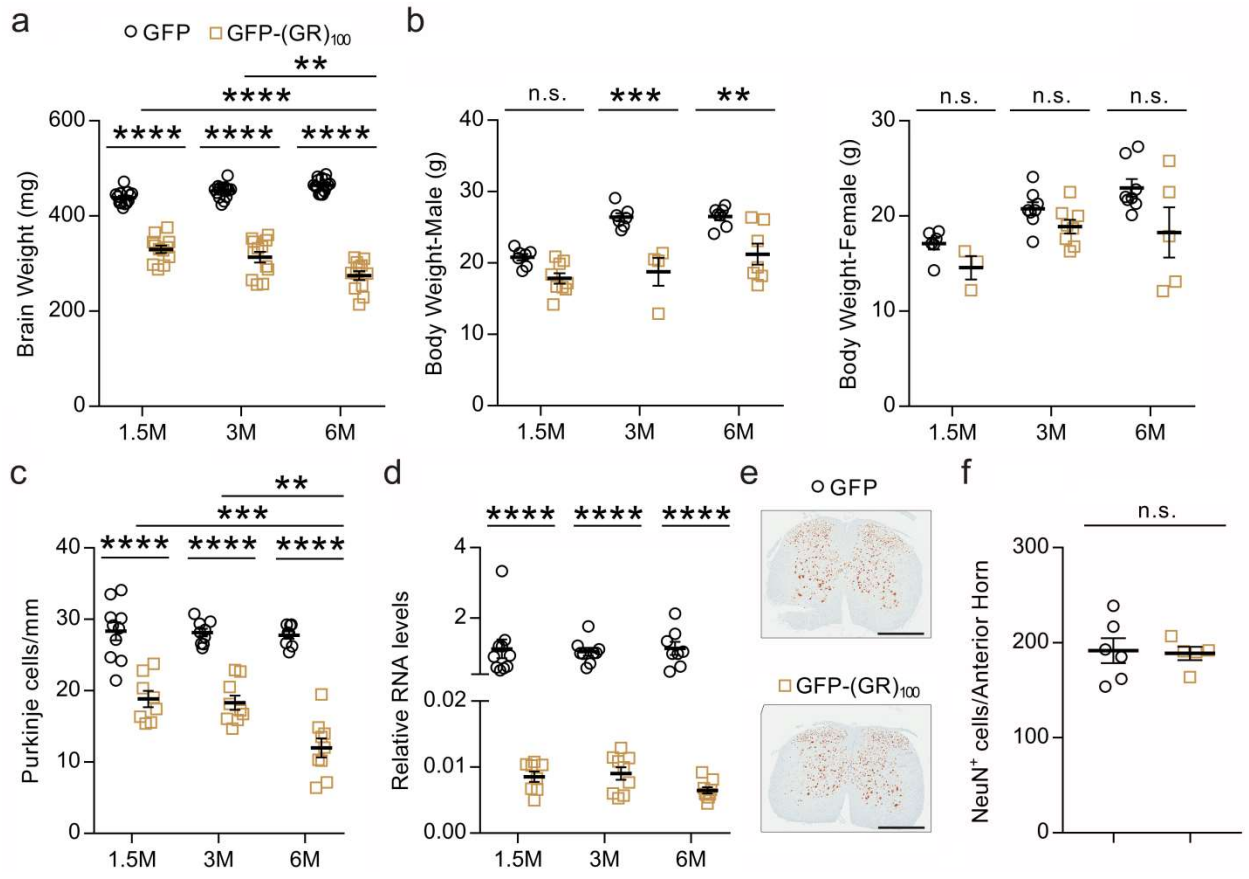

Supplementary Figure 4. GFP-(GR)$_{100}$ mice developed neurodegeneration. (**a**) Mean brain weight of 1.5-, 3- and 6-month-old mice expressing GFP (n = 13, 15, 15, respectively) or GFP-(GR)$_{100}$ (n = 12 per group). (**b**) Mean body weight of 1.5-, 3- and 6-month-old male mice expressing GFP (n = 7 per group) or GFP-(GR)$_{100}$ (n = 9, 4, 7, respectively); or of 1.5-, 3- and 6-month-old female mice expressing GFP (n = 6, 8, 8, respectively) or GFP-(GR)$_{100}$ (n = 3, 8, 5, respectively). (**c**) Quantification of the number of Purkinje cells within an annotated area of the cerebellum of 1.5-, 3- and 6-month-old mice expressing GFP (n = 10, 9, 8, respectively) or GFP-(GR)$_{100}$ (n = 8, 9, 9, respectively). (**d**) Quantitative real-time PCR analysis of transgene RNA using RNA extracted from the cortex and hippocampus of 1.5-, 3- and 6-month-old mice expressing GFP (n = 10, 9, 8, respectively) or GFP-(GR)$_{100}$ (n = 8, 9, 9, respectively). (**e**,**f**)

Representative images (**e**) and quantification of NeuN-labeled cells in the spinal cord (**f**) of 6-month-old mice expressing GFP (n = 6) or GFP-$(GR)_{100}$ (n = 5). Scale bars, 600 μm. Data are presented as mean±s.e.m. In **a**: **** $P < 0.0001$ and ** $P = 0.0037$, two-way ANOVA, Tukey's multiple-comparison test. In **b**: *** $P = 0.0002$, ** $P = 0.0038$, n.s. (left to right) $P = 0.1806$, $P = 0.8080$, $P = 0.7772$ and $P = 0.0715$, two-way ANOVA, Tukey's multiple-comparison test. In **c**: **** $P < 0.0001$, *** $P = 0.0006$ and ** $P = 0.0012$, two-way ANOVA, Tukey's multiple-comparison test. In **d**: **** $P < 0.0001$, two-way ANOVA, Tukey's multiple-comparison test. In **f**: n.s. $P = 0.8607$, two-tailed unpaired t test. n.s., not significant.

Supplementary Figure 5

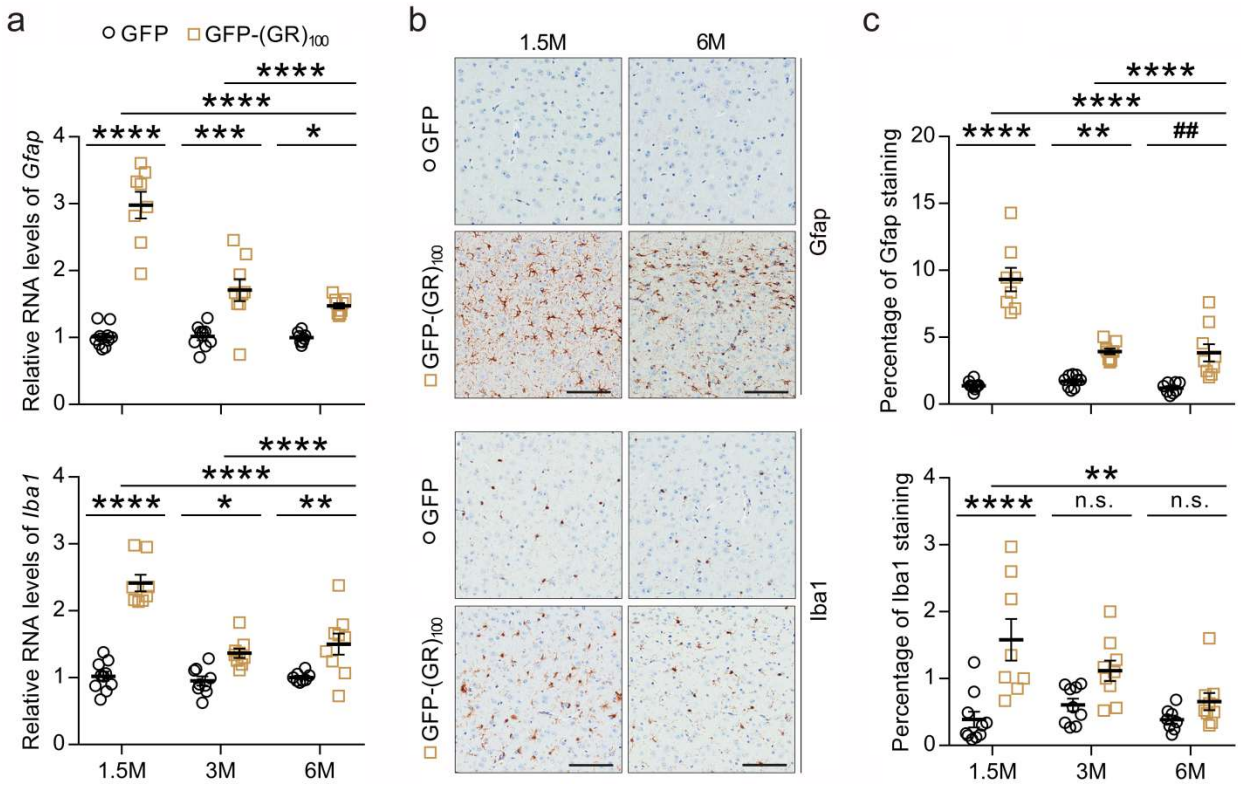

Supplementary Figure 5. GFP-(GR)$_{100}$ mice developed gliosis. (**a**) Quantitative real-time PCR analysis of relative RNA levels of the astrocyte marker *Gfap* (top) and the microglia marker *Iba1* (bottom) using RNA extracted from the cortex and hippocampus of 1.5-, 3- and 6-month-old mice expressing GFP (n = 10, 9, 8, respectively) or GFP-(GR)$_{100}$ (n = 8, 9, 9, respectively). (**b**) Representative images of Gfap (top) or Iba1 (bottom) staining in the cortex of 1.5- and 6-month-old mice expressing GFP (n = 10, 8, respectively) or GFP-(GR)$_{100}$ (n = 8, 9, respectively). Scale bars, 100 μm. (**c**) Quantification of astrogliosis (top) and microgliosis (bottom), analyzed by measuring Gfap- or Iba1-positivity in the cortex of 1.5-, 3- and 6-month-old mice expressing GFP (n = 10, 9, 8, respectively) or GFP-(GR)$_{100}$ (n = 8, 9, 9, respectively) using a positive pixel count algorithm. Data are presented as mean±s.e.m. In **a**: top, **** $P < 0.0001$, *** $P = 0.0004$ and * $P = 0.0404$, two-way ANOVA, Tukey's multiple-comparison test; bottom, **** $P <$

0.0001, ** $P = 0.0088$ and * $P = 0.0353$, two-way ANOVA, Tukey's multiple-comparison test. In **c**: top, **** $P < 0.0001$, ** $P = 0.0095$ and $^{\#\#}$ $P = 0.0018$, two-way ANOVA, Tukey's multiple-comparison test; bottom, **** $P < 0.0001$, ** $P = 0.0024$ and n.s. (left to right) $P = 0.2138$ and $P = 0.8467$, two-way ANOVA, Tukey's multiple-comparison test. n.s., not significant.

Supplementary Figure 6

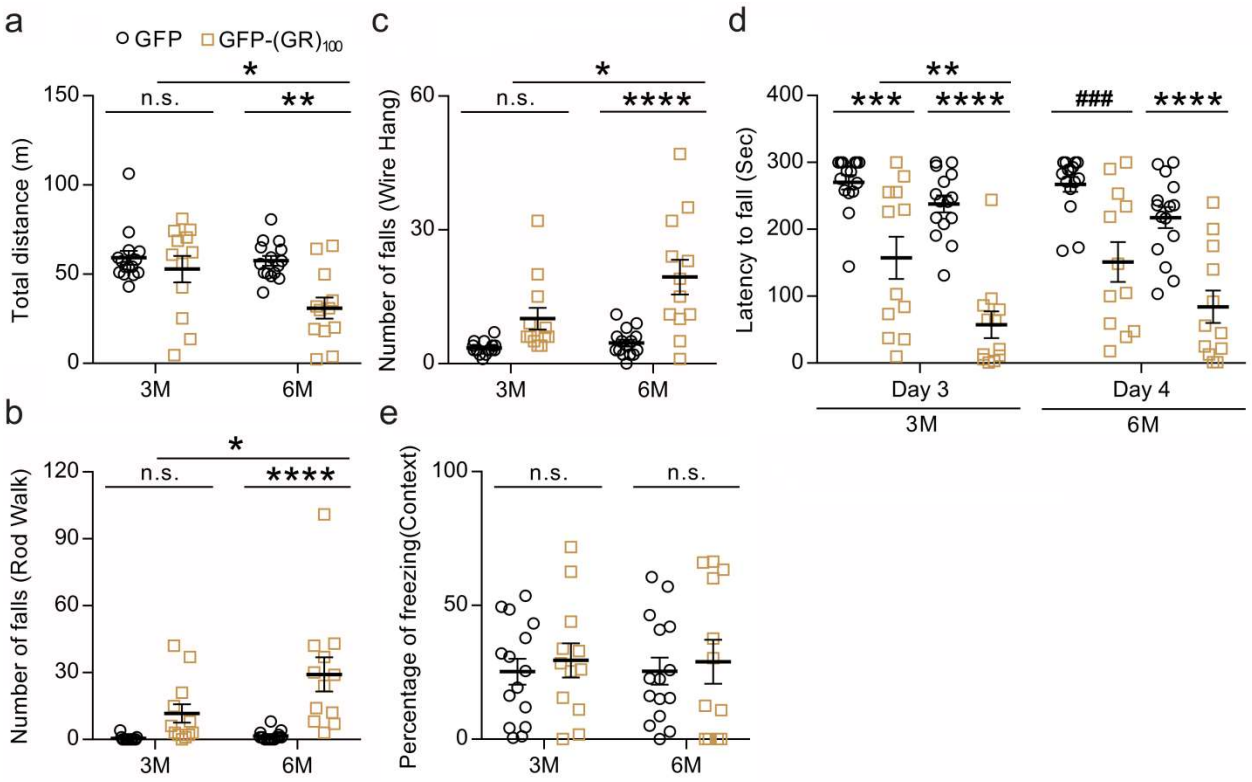

Supplementary Figure 6. GFP-$(GR)_{100}$ mice developed motor and cognitive deficits. (**a**) Results from the open field test analyzing the behavior of 3- and 6-month-old mice expressing GFP (n = 15 per group) or GFP-$(GR)_{100}$ (n = 12 per group), where locomotive defects were indicated by a decrease in total distance traveled. (**b**,**c**) Results from the rod walk (**b**) and wire hang (**c**) tests analyzing motor function of 3- and 6-month-old mice expressing GFP (n = 15 per group) or GFP-$(GR)_{100}$ (n = 12 per group) by evaluating the number of falls. (**d**) Day 3 and day 4 results from a four day rotarod test used to determine motor deficits of 3- and 6-month-old mice expressing GFP (n = 15 per group) or GFP-$(GR)_{100}$ (n = 12 per group) by evaluating latency to fall from a rotating rod (see also **Fig. 1h** for day 1 and day 2 results). (**e**) In the contextual fear conditioning test, associative learning and memory of mice expressing GFP (n = 15 per group) or GFP-$(GR)_{100}$ (n = 12 per group) were evaluated by the percent of time mice spent frozen in response to being placed in the environment that had previously been paired with a foot shock.

Data are presented as mean±s.e.m. In **a**: ** $P = 0.0024$, * $P = 0.0241$ and n.s. $P = 0.8094$, two-way ANOVA, Tukey's multiple-comparison test. In **b**: **** $P < 0.0001$, * $P = 0.0205$ and n.s. $P = 0.1859$, two-way ANOVA, Tukey's multiple-comparison test. In **c**: **** $P < 0.0001$, * $P = 0.0217$ and n.s. $P = 0.1280$, two-way ANOVA, Tukey's multiple-comparison test. In **d**: **** $P < 0.0001$, *** $P = 0.0006$, ### $P = 0.0004$ and ** $P = 0.0051$, two-way ANOVA, Tukey's multiple-comparison test. In **e**: n.s. (left to right) $P = 0.9610$ and $P = 0.9766$, two-way ANOVA, Tukey's multiple-comparison test. n.s., not significant.

Supplementary Figure 7

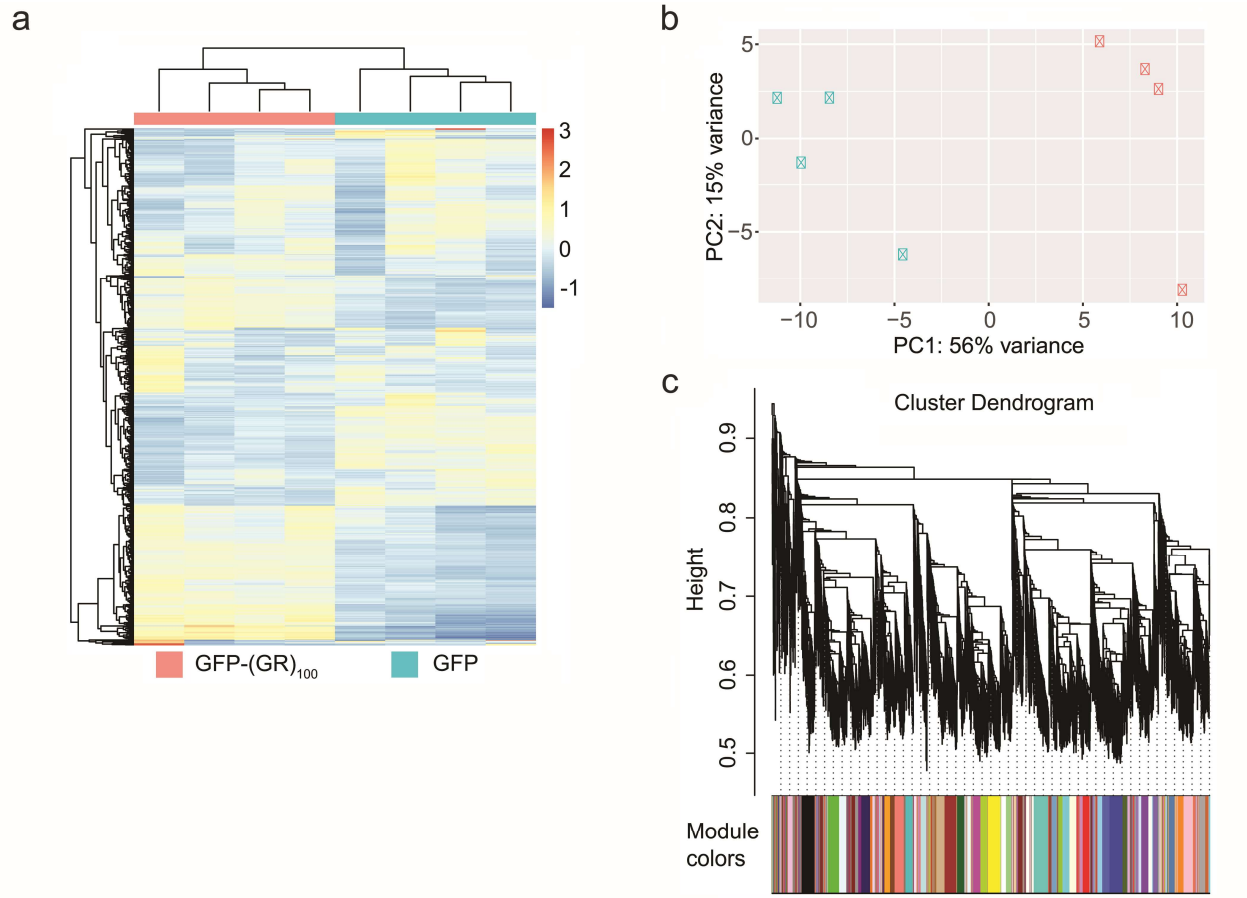

Supplementary Figure 7. Transcriptome alterations were identified in brains of mice expressing GFP-$(GR)_{100}$. (**a**) Hierarchical clustering of the 1000 most variable genes between 1.5-month-old GFP and GFP-$(GR)_{100}$ mice (n = 4 per group). (**b**) Principal-component analyses to determine divergence between 1.5-month-old GFP and GFP-$(GR)_{100}$ mice (n = 4 per group). (**c**) Gene modules identified in brains of 1.5-month-old mice expressing GFP-$(GR)_{100}$ (n = 4) through weighted gene-coexpression correlation network analyses using differentially-expressed genes.

Supplementary Figure 8.

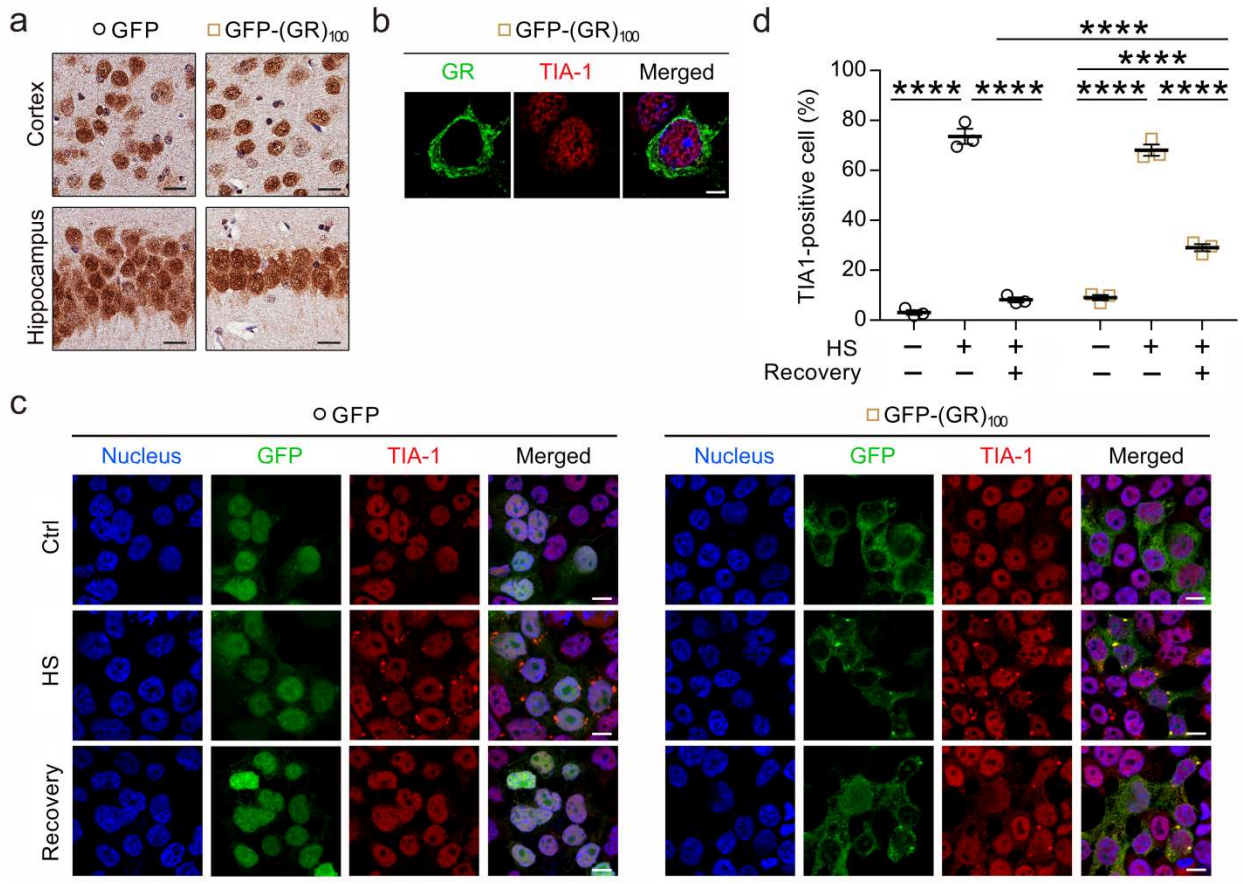

Supplementary Figure 8. Diffuse GFP-$(GR)_{100}$ was recruited into stress granules formed in response to heat shock, and impaired their disassembly during the recovery phase. (**a**) Immunohistochemical analysis of TIA-1 in the cortex and hippocampus of 6-month-old mice expressing GFP or GFP-$(GR)_{100}$ (n = 3 per group). Scale bars, 20 μm. (**b**) Double-immunofluorescence staining for poly(GR) and TIA-1 in the cortex of 6-month-old mice expressing GFP-$(GR)_{100}$ (n = 3). Scale bars, 5 μm. (**c**) Double-immunofluorescence staining for TIA-1 and either GFP or GFP-$(GR)_{100}$ in HEK293T cells expressing GFP or diffuse GFP-$(GR)_{100}$ under basal (Ctrl), heat shock (HS) or post-heat shock conditions (Recovery) (n = 3 independent experiments). (**d**) Quantification of the percentage of GFP- or GFP-$(GR)_{100}$-expressing HEK293T cells containing TIA-1-positive stress granules under basal, heat shock (HS)

or post-heat shock conditions (Recovery) (n = 3 independent experiments). Scale bars, 10 μm. Data are presented as mean±s.e.m. In **b**: **** $P < 0.0001$, two-way ANOVA, Tukey's multiple-comparison test.

Supplementary Figure 9.

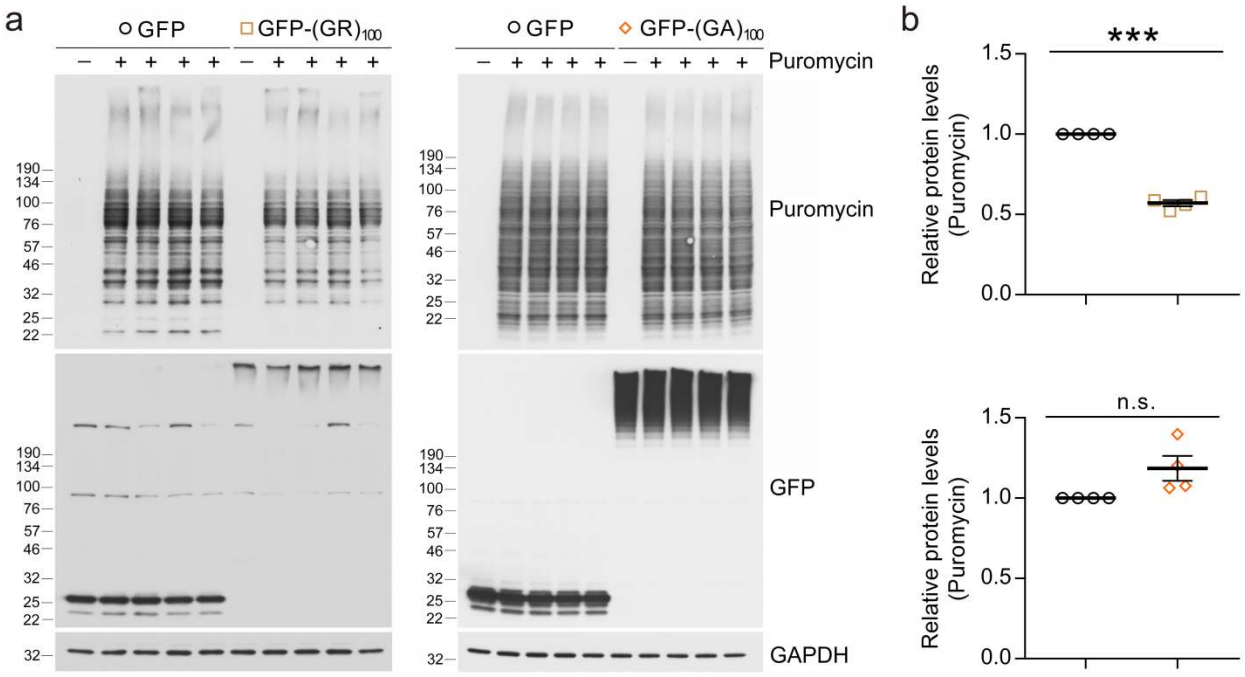

Supplementary Figure 9. Expression of GFP-$(GR)_{100}$, but not GFP-$(GA)_{100}$, impaired canonical translation. (**a**,**b**) Immunoblots (**a**) and densitometric analysis of immunoblots (**b**) for the indicated proteins to examine the production of nascent proteins labeled with puromycin in HEK293T cells expressing GFP versus GFP-$(GR)_{100}$ (n = 4 independent experiments), and GFP versus GFP-$(GA)_{100}$ (n = 4 independent experiments). Data are presented as mean±s.e.m. In **b**: **** $P < 0.0001$ and n.s. $P = 0.0540$, two-tailed unpaired t test. n.s., not significant.

Supplementary Figure 10.

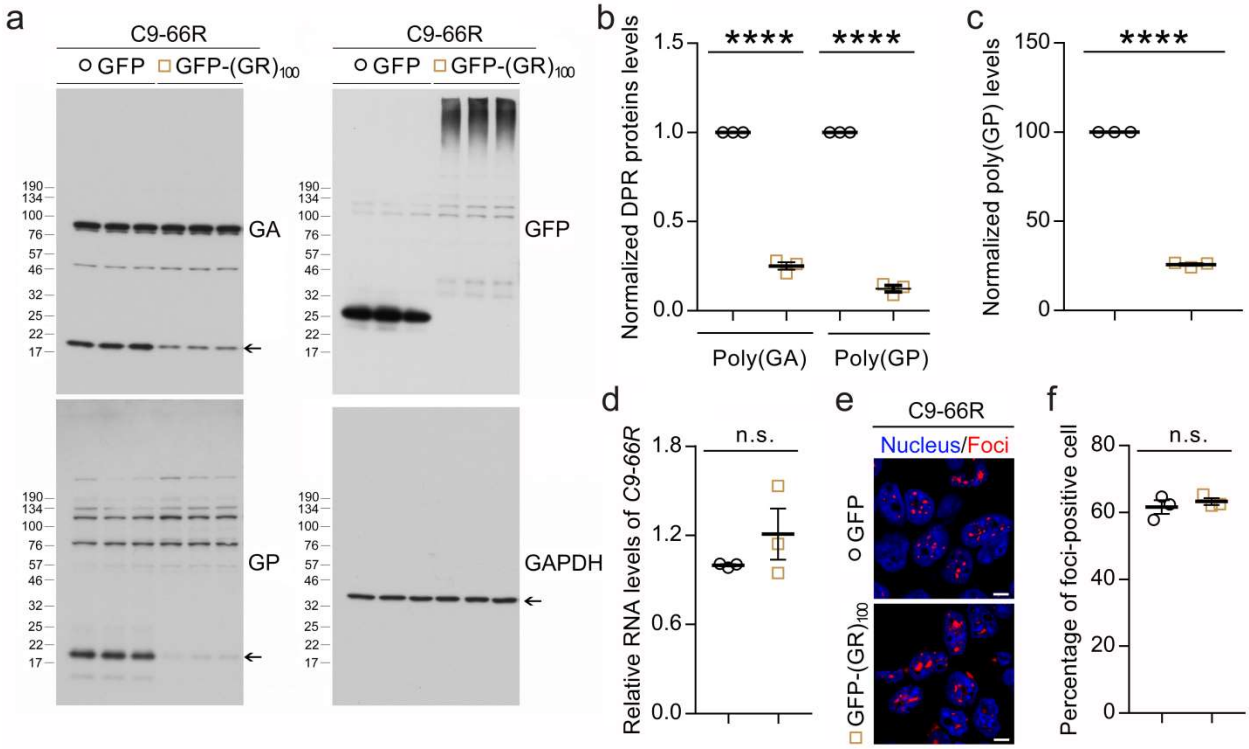

Supplementary Figure 10. Expression of GFP-$(GR)_{100}$ inhibited repeat-associated non-ATG translation of *C9orf72* G_4C_2 repeat expansions. (**a**,**b**) Full Western blots from **Fig. 4h** (**a**) and densitometric analysis (**b**) of immunoblots for poly(GA) and poly(GP) RAN translated in HEK293T cells co-expressing $(G_4C_2)_{66}$ and either GFP or GFP-$(GR)_{100}$ (n = 3 independent experiments). Arrows indicate bands from cropped blots shown in **Fig. 4h**. (**c**) Levels of RAN translated poly(GP) in HEK293T cells co-expressing $(G_4C_2)_{66}$ and either GFP or GFP-$(GR)_{100}$, as assessed by immunoassay (n = 3 independent experiments). (**d**) Quantitative real-time PCR analysis of relative RNA levels of $(G_4C_2)_{66}$ (C9-66R) in HEK293T cells co-expressing $(G_4C_2)_{66}$ and either GFP or GFP-$(GR)_{100}$ (n = 3 independent experiments). (**e**) RNA FISH to detect nuclear foci containing G_4C_2 repeat RNA in HEK293T cells co-expressing $(G_4C_2)_{66}$ (C9-66R) and either GFP or GFP-$(GR)_{100}$ (n = 3 independent experiments). Scale bars, 5 μm. (**f**) Quantitation of the percentage of cells containing nuclear RNA foci (n = 3 independent

experiments). Data are presented as mean±s.e.m. In **b** and **c**: **** $P < 0.0001$, two-tailed unpaired t test. In **d**: n.s. $P = 0.2898$, two-tailed unpaired t test. In **f**: n.s. $P = 0.5095$, two-tailed unpaired t test. n.s., not significant.

Supplementary Figure 11.

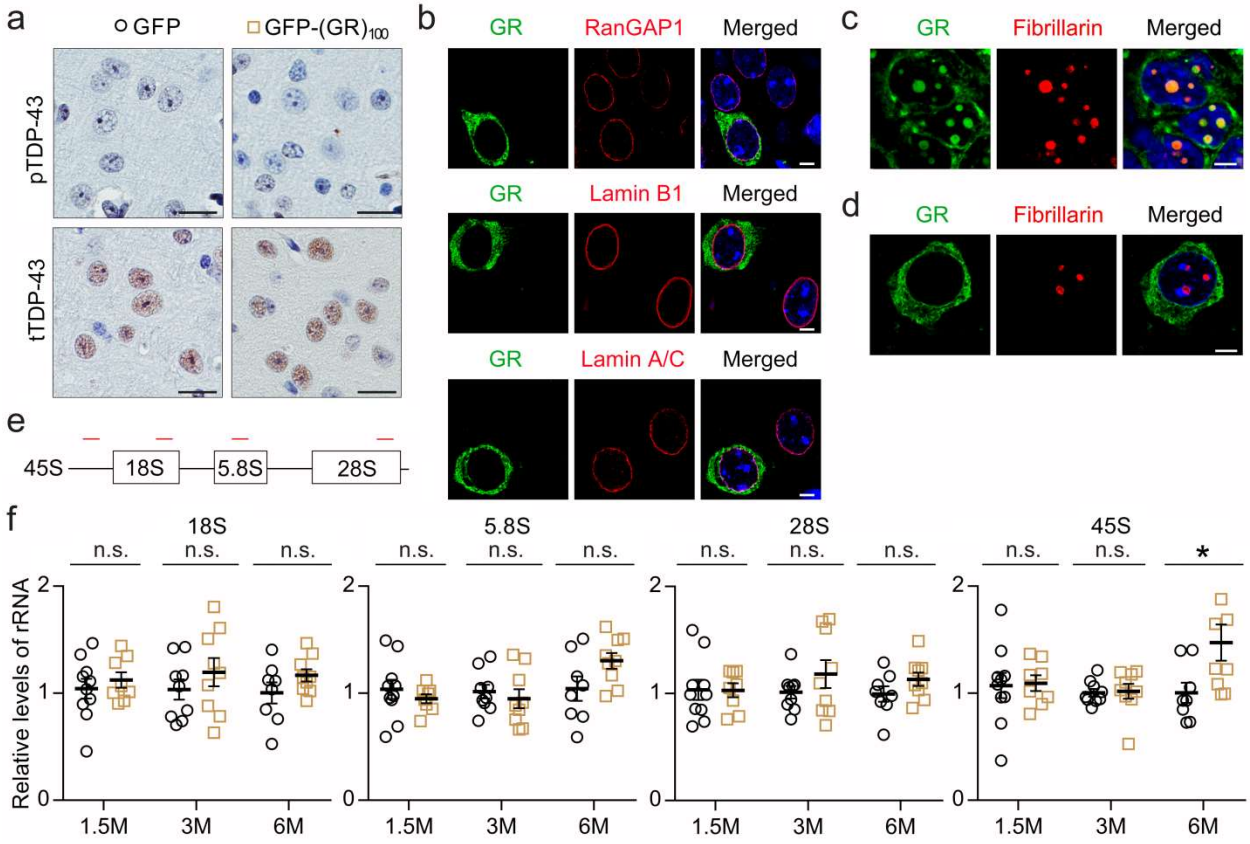

Supplementary Figure 11. Expression of GFP-$(GR)_{100}$ in mice did not cause TDP-43 pathology, impaired nuclear membrane integrity or nucleolar stress. (**a**) Immunohistochemical analysis using antibodies to detect TDP-43 phosphorylated at serine residues 409 and 410 (pTDP-43) or total TDP-43 (tTDP-43) in the cortex of 6-month-old mice expressing GFP or GFP-$(GR)_{100}$ (n = 5 per group). Scale bars, 20 μm. (**b**) Double-immunofluorescence staining for GFP-$(GR)_{100}$ and RanGAP1, lamin B1 or lamin A/C in the cortex of 6-month-old mice expressing GFP-$(GR)_{100}$ (n = 5). Scale bar, 5 μm. (**c**,**d**) Double-immunofluorescence staining for GFP-$(GR)_{100}$ and the nucleolar marker fibrillarin in HEK293T cells (**c**, n = 3 independent experiments) or in the cortex of 6-month-old mice expressing GFP-$(GR)_{100}$ (**d**, n = 5). Scale bar, 5 μm. (**e**) Schematic representation of ribosomal RNA (rRNA) and the regions to which primers were designed for quantitative real-time PCR analysis (qPCR). (**f**)

qPCR analysis of relative levels of 45S, 18S, 5.8S and 28S rRNA in brains of 1.5-, 3- and 6 month-old mice expressing GFP (n = 10, 9, 8, respectively) or GFP-$(GR)_{100}$ (n = 8, 9, 9, respectively). Data are presented as mean±s.e.m. In **f**: * P = 0.0363 and n.s. (left to right) P = 0.9905, P = 0.8210, P = 0.8361, P = 0.9730, P = 0.9916, P = 0.2512, P > 0.9999, P = 0.7280, P = 0.8771, P > 0.9999 and P > 0.9999, two-way ANOVA, Tukey's multiple-comparison test. n.s., not significant.

Supplementary Figure 12.

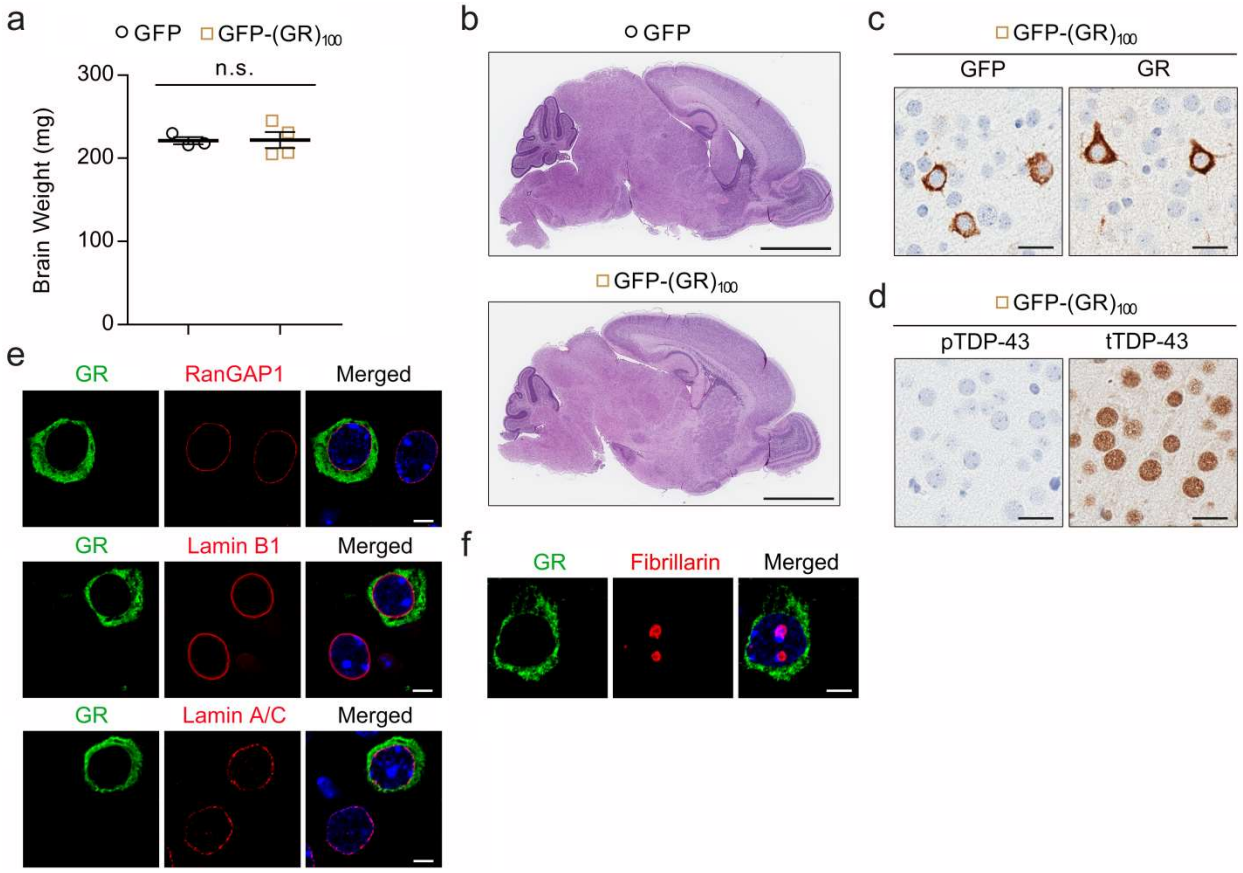

Supplementary Figure 12. Characterization of the cellular distribution of GFP-$(GR)_{100}$, TDP-43 pathology, and nuclear membrane integrity in 1-week-old GFP-$(GR)_{100}$ mice. (**a**) Mean brain weight of 1-week-old mice expressing GFP (n = 3) or GFP-$(GR)_{100}$ (n = 4). (**b**) Gross morphological analysis with hematoxylin and eosin staining of brains from 1-week-old mice expressing GFP (n = 3) or GFP-$(GR)_{100}$ (n = 4). Scale bar, 2 mm. (**c**) Immunohistochemical analysis using antibodies to detect GFP or poly(GR) in the cortex of 1-week-old mice expressing GFP-$(GR)_{100}$ (n = 4). Scale bars, 20 μm. (**d**) Immunohistochemical analysis using antibodies to detect TDP-43 phosphorylated at serine residues 409 and 410 (pTDP-43) or total TDP-43 (tTDP-43) in the cortex of 1-week-old mice expressing GFP-$(GR)_{100}$ (n = 4). Scale bars, 20 μm. (**e**) Double-immunofluorescence staining for GFP-$(GR)_{100}$ and

RanGAP1, lamin B1 or lamin A/C in the cortex of 1-week-old mice expressing GFP-$(GR)_{100}$ (n = 4). Scale bar, 5 μm. (**f**) Double-immunofluorescence staining for GFP-$(GR)_{100}$ and the nucleolar marker fibrillarin in the cortex of 1-week-old mice expressing GFP-$(GR)_{100}$ (n = 4). Scale bar, 5 μm. Data are presented as mean±s.e.m. In **a**: n.s. P = 0.9579, two-tailed unpaired t test. n.s., not significant.

Supplementary Table 1a. cDNA sequence of the GFP-$(GR)_{100}$ plasmid

ATGGTGAGCAAGGGCGAGGAGCTGTTCACCGGGGTGGTGCCCATCCTGGTCGAGCT
GGACGGCGACGTAAACGGCCACAAGTTCAGCGTGTCCGGCGAGGGCGAGGGCGAT
GCCACCTACGGCAAGCTGACCCTGAAGTTCATCTGCACCACCGGCAAGCTGCCCGTG
CCCTGGCCCACCCTCGTGACCACCCTGACCTACGGCGTGCAGTGCTTCAGCCGCTAC
CCCGACCACATGAAGCAGCACGACTTCTTCAAGTCCGCCATGCCCGAAGGCTACGTC
CAGGAGCGCACCATCTTCTTCAAGGACGACGGCAACTACAAGACCCGCGCCGAGGT
GAAGTTCGAGGGCGACACCCTGGTGAACCGCATCGAGCTGAAGGGCATCGACTTCA
AGGAGGACGGCAACATCCTGGGGCACAAGCTGGAGTACAACTACAACAGCCACAA
CGTCTATATCATGGCCGACAAGCAGAAGAACGGCATCAAGGTGAACTTCAAGATCC
GCCACAACATCGAGGACGGCAGCGTGCAGCTCGCCGACCACTACCAGCAGAACACC
CCCATCGGCGACGGCCCCGTGCTGCTGCCCGACAACCACTACCTGAGCACCCAGTCC
GCCCTGAGCAAAGACCCCAACGAGAAGCGCGATCACATGGTCCTGCTGGAGTTCGT
GACCGCCGCCGGGATCACTCTCGGCATGGACGAGCTGTACAAGTCCGGACTCAGAT
CTCGAGCTCAAGCTTCG**GGCCGCGGCCGTGGTCGCGGTCGTGGACGTGGCCGTGGC**
CGTGGCCGAGGTCGCGGTCGGGGACGTGGCCGTGGTCGTGGCCGAGGTCGAGGTCG
CGGACGTGGACGTGGTCGAGGTCGGGGACGTGGACGAGGCCGTGGTCGTGGCCGAG
GTCGCGGACGTGGGCGAGGTCGCGGTCGAGGCCGGGGACGTGGCCGTGGTCGTGGA
CGGGGACGGGGTCGGGGACGCGGTCGAGGCCGTGGACGTGGACGGGGTCGAGGAC
GTGGACGTGGTCGTGGACGTGGCCGTGGACGTGGACGCGGCCGTGGTCGCGGTCGT
GGACGTGGCCGTGGCCGTGGCCGAGGTCGCGGTCGGGGACGTGGCCGTGGTCGTGG
CCGAGGTCGAGGTCGCGGACGTGGACGTGGTCGAGGTCGGGGACGTGGACGAGGCC
GTGGTCGTGGCCGAGGTCGCGGACGTGGGCGAGGTCGCGGTCGAGGCCGGGGACGT
GGCCGTGGTCGTGGACGGGGACGGGGTCGGGGACGCGGTCGAGGCCGTGGACGTGG
ACGGGGTCGAGGACGTGGACGTGGTCGTGGACGTGGCCGTGGACGTGGACGGTAG

The $(GR)_{100}$ sequence is highlighted in yellow.

Supplementary Table 1b. Primary antibodies for immunohistochemistry and immunofluorescence staining

Antibody	Species	Dilution	Number	Company
anti-GFP	rabbit	1:1000	A-6455	Life Technologies
anti-GFP	mouse	1:2000	33-2600	Thermo Fisher Scientific
anti-GR	rabbit	1:2000	Rb7810[a]	
anti-NeuN	mouse	1:5000	MAB377	Chemicon International
anti-GFAP	rabbit	1:2500	PU020-UP	Biogenex
anti-Iba1	rabbit	1:3000	019-19741	Wako Chemicals
anti-Fibrillarin	mouse	1:1000	ab4566	Abcam
anti-GA	mouse	1:1000	MABN889	EMD Millipore
anti-S6	mouse	1:100	2317S	Cell Signaling
anti-L21	mouse	1:100	sc-393663	Santa Cruz Biotechnology
anti-eIF3η	goat	1:200	sc-16377	Santa Cruz Biotechnology
anti-eIF3η	mouse	1:200	sc-137214	Santa Cruz Biotechnology
anti-S25	rabbit	1:100	NBP1-80802	Novus Biologicals
anti-Tom20	mouse	1:200	sc-17764	Santa Cruz Biotechnology
anti-KDEL	mouse	1:250	SPA-827	Stressgen
anti-TIA-1	goat	1:100	sc-1751	Santa Cruz Biotechnology
anti-puromycin	mouse	1:1000	MABE342	EMD Millipore
anti-TDP-43	rabbit	1:2000	12892-1-AP	Proteintech
anti-pTDP-43	rabbit	1:1000	Rb3655[b]	
anti-RanGAP1	rabbit	1:100	sc-25630	Santa Cruz Biotechnology
anti-Lamin B1	rabbit	1:100	ab133741	Abcam
anti-Lamin A/C	goat	1:100	sc-6215	Santa Cruz Biotechnology

[a]Antibody described in: Gendron, T.F., *et al*. Antisense transcripts of the expanded C9ORF72 hexanucleotide repeat form nuclear RNA foci and undergo repeat-associated non-ATG translation in c9FTD/ALS. *Acta Neuropathol*. 126, 829-844 (2013).

[b]Antibody described in: Chew, J.*, et al.* Neurodegeneration. C9ORF72 repeat expansions in mice cause TDP-43 pathology, neuronal loss, and behavioral deficits. *Science.* 348, 1151-1154 (2015).

Supplementary Table 1c. Primers

Model	Target	Primers
mouse brain	45S rRNA	5’-GAGTTCACGGTGGGTTCG-3’
		5’-GAGAAGACCACGCCAACG-3’
mouse brain	18S rRNA	5’- GTAACCCGTTGAACCCCATT-3’
		5’-CCATCCAATCGGTAGTAGCG-3’
mouse brain	5.8S rRNA	5’-CTCGTGCGTCGATGAAGAA-3’
		5’-TCGAAGTGTCGATGATCAATGT-3’
mouse brain	28S rRNA	5’-ATATCCGCAGCAGGTCTCC-3’
		5’-GCCGACTTCCCTTACCTACA-3’
mouse brain	*GFP*	5′-GAAGCGCGATCACATGGT-3′
		5′-CCATGCCGAGAGTGATCC-3′
mouse brain	*Gfap*	5’-GGAGAGGGACAACTTTGCAC-3’
		5’-AGCCTCAGGTTGGTTTCATC-3’
mouse brain	*Iba1*	5’-GGATTTGCAGGGAGGAAAAG-3’
		5’- TGGGATCATCGAGGAATTG-3’
mouse brain	*Gadph*	5′-CATGGCCTTCCGTGTTCCTA-3′
		5′-CCTGCTTCACCACCTTCTTGAT-3’
cultured HEK293T cells	*C9-66R*	5’-TACAGCTCCTGGGCAACG-3’
		5’-CTTGTTCACCCTCAGCGAGT-3’
cultured HEK293T cells	*GAPDH*	5’-GTTCGACAGTCAGCCGCATC-3’
		5’-GGAATTTGCCATGGGTGGA-3’

Supplementary Table 2. Patient Characteristics

Case #	Pathological Diagnosis	Gender	Age at Onset	Age at death	Disease Duration	*C9orf72* repeat expansion
1	FTD	Male	63	66	3.1	Yes
2	FTD	Male	55	61	6.2	Yes
3	FTD	Male	n.a.	64	n.a.	Yes
4	FTD	Male	68	73	5.9	Yes
5	FTD	Male	n.a.	65	n.a.	Yes
6	FTD	Male	n.a.	66	n.a.	Yes
7	ALS	Female	41	42	1.3	Yes
8	FTD-ALS	Female	n.a.	51	n.a.	Yes
9	FTD-ALS	Female	49	52	2.7	Yes
10	ALS	Female	48	49	1.1	Yes
11	FTD	Female	44	56	12.2	Yes
12	FTD-ALS	Female	52	60	8.3	Yes
13	FTD	Male	55	63	8.6	Yes
14	FTD	Male	63	67	3.9	No
15	FTD	Female	79	87	8.3	No

FTD, frontotemporal degeneration; ALS, amyotrophic lateral sclerosis; n.a., not available;
Cases #1 to #8 were used for immunochemistry and immunofluorescence staining, and cases #9 to #15 were used for immunoassay.